nature materials

SUPPLEMENTARY INFORMATION

DOI: 10.1038/NMAT4479

A new active Li–Mn–O compound for high energy density Li-ion batteries

M. Freire[a,c], N.V. Kosova[b], C. Jordy[c], D. Chateigner[a], O.I. Lebedev[a], A. Maignan[a] and V. Pralong[a]*

[a] *Laboratoire de Cristallographie et Sciences des Matériaux CRISMAT, ENSICAEN, Université de Caen, CNRS, 6 Bd Maréchal Juin, F-14050 Caen, France.*

[b] *Institute of Solid State Chemistry and Mechanochemistry SB RAS, 18 Kutateladze, Novosibirsk 630128, Russia.*

[c] *Saft, Direction de la Recherche, 111/113 Bd Alfred Daney, 33074 Bordeaux, France.*

DOI: 10.1038/NMAT4479

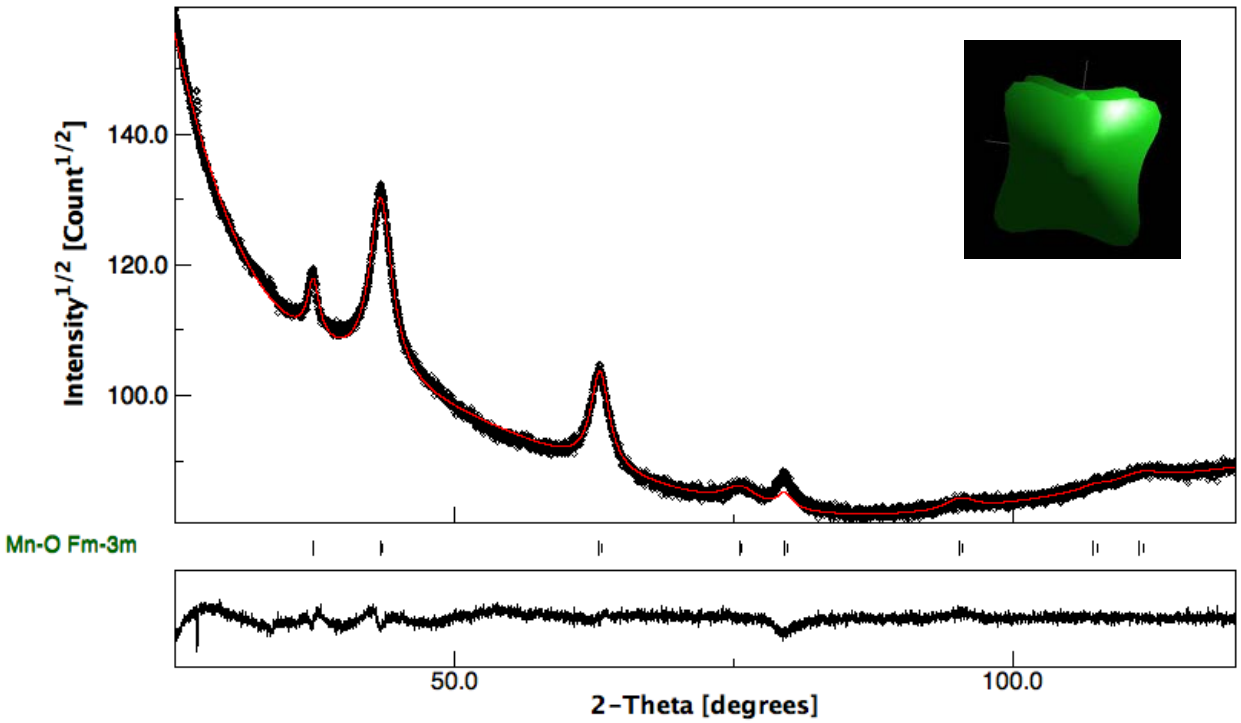

Figure S1. X-ray diffraction Rietveld fit using the MAUD software: GoF = 1.53; R_{wp} = 1.58 %; R_{Bragg} = 1.23 %; $R_{expected}$ = 1.03 %. These results are obtained using a Popa-like mean anisotropic crystallite sizes and microstrain model up to a harmonic expansion L=8, which gives a mean size along the [100] direction of 46(1)Å, and 81(2)Å along [111] (see insert of Figure S1). The corresponding microstrains are not larger than 1.6 10^{-4} rms and 5.5 10^{-3} rms, indicating a slightly larger disorder along the cube diagonals. Even if the reliability factors point to a reasonably good fit, we cannot assume that this as a final solution, peculiarly since Li content was not incorporated in the unit-cell, i.e. not refined in this experiment. However the unit-cell parameter a=4.1732(9)Å can reasonably be fitted. An isotropic atomic displacement parameter was also fitted to Biso=0.51(6) and 0.74(13) for Mn and O respectively, but these latter are much more sensitive to initial fit conditions, and rapidly reach unphysical values in our experimental set.

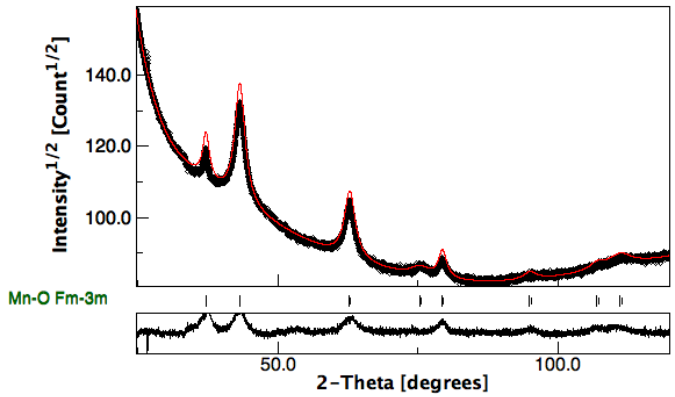

a)

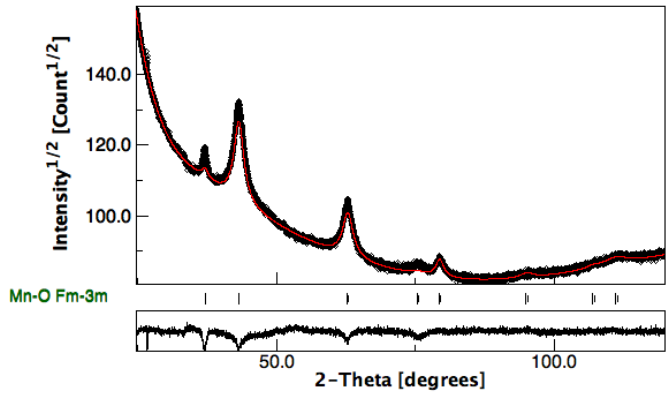

b)

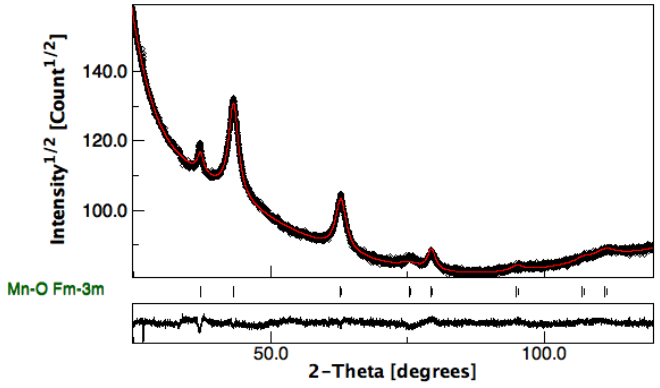

c)

Figure S2. X-ray diffraction Rietveld fits with Li substituted for Mn, modeled with Mn/Li = 0.6/0.4 (a), 0.4/0.6 (b) and fitted to 0.48(1)/0.52(1) (c; GoF = 1.24). The first (111) and the 2θ=75° (311) peaks are the most affected by Li substitution in this Fm-3m structure, but a 20% variation in Mn/Li does not result in a noticeable modification of diagram (compare Figures S2 a and b). A fit could accommodate a roughly 0.5/0.5 Li/Mn ratio (Figure S2c), however with large uncertainties due to eventual secondary phases. The cell parameter enlarges to a=4.1824(6) during this fit, which still is acceptable in front of the strong line broadening (the crystallite size does not vary significantly compared to the fit of Figure S1). Please note on the fly that the line profile is strongly Cauchy-like, i.e. due to a size effect and not to large microstrains in the crystals.

DOI: 10.1038/NMAT4479

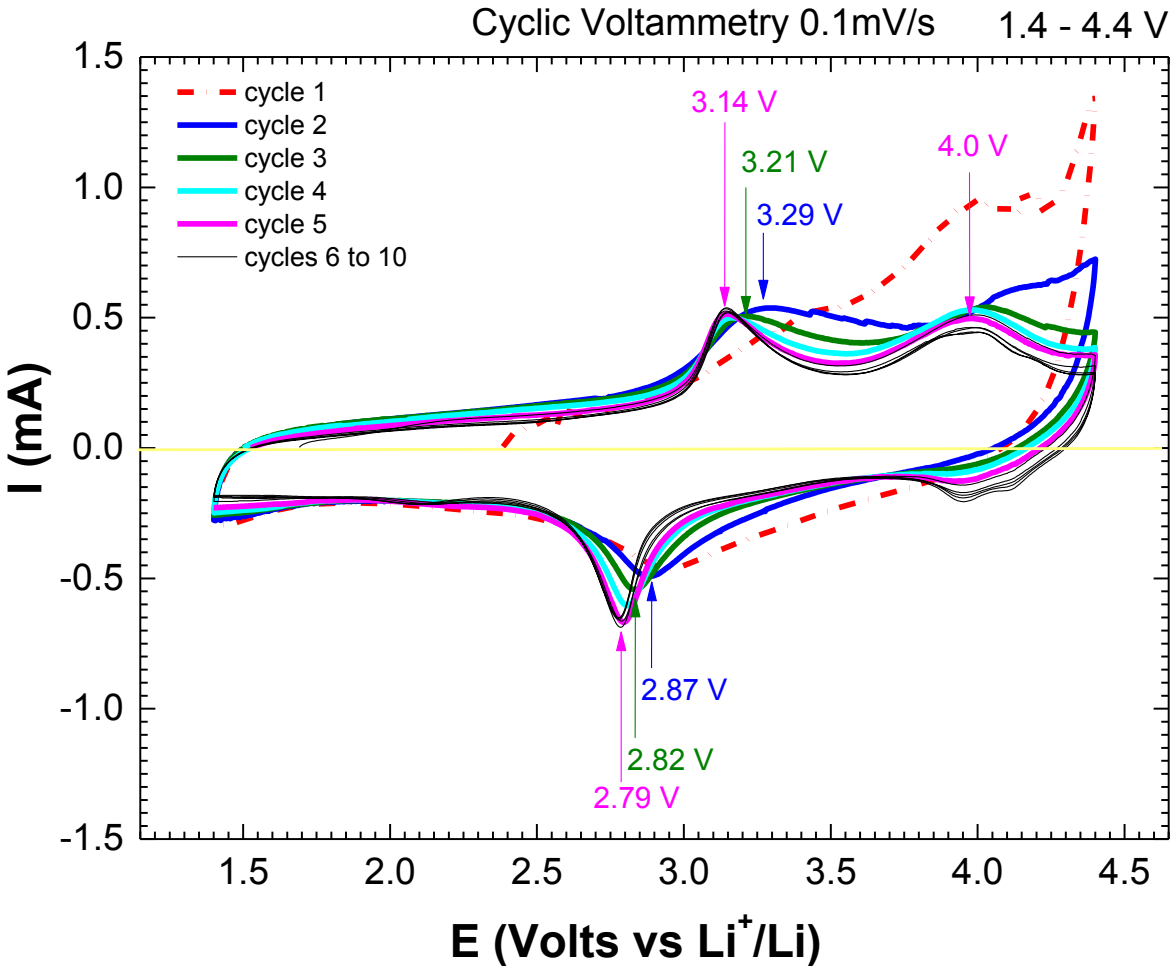

Figure S3. Cyclic voltammetry curves of $Li_4Mn_2O_5$. During the first cycle (red dashed line), redox processes are observed during the oxidation at high potential (between 4 - 4.4V). From the second cycle, electrochemical peaks maintained unchanged: during the charge, the first process (3.29V) corresponds to the oxidation of Mn^{+3} in Mn^{+4} and the second redox process, which occurs at 4.1V, is attributed to the oxidation of Mn^{+4} to Mn^{+5} and/or the oxygen oxidation (O^{2-}/O^{-} and/or O^{-}/O_2). During the reduction, broad peaks around 4V (probably Mn^{5+}/Mn^{4+}) and the peak at 2.87V correspond to the reduction of Mn^{+4} to Mn^{+3}.

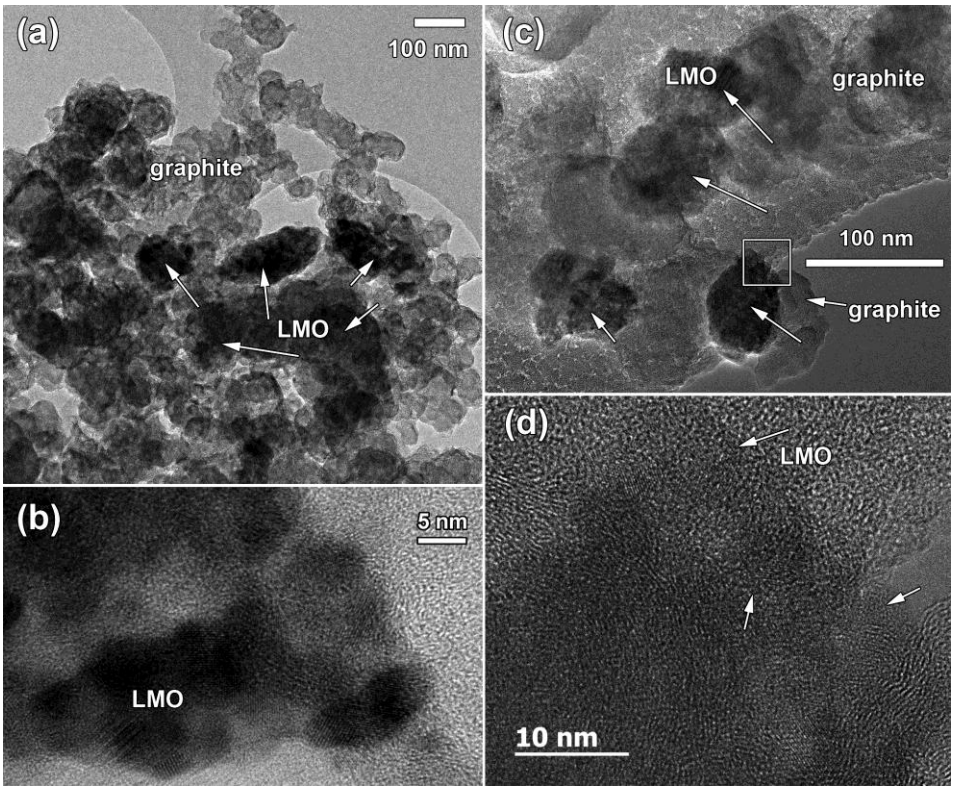

Figure S4. (a) - Bright field low magnification and (b)- HRTEM images of the '$Li_{4-x}Mn_2O_5$' nanoparticles after one cycle on the discharged state. (c) - Bright field low magnification and (d)- HRTEM images of the '$Li_{4-x}Mn_2O_5$' nanoparticles after three cycles on the discharged state. Notice graphitic layers (light dark contrast) mixed with agglomerate of LMO nanoparticles (dark contrast) marked by white arrows. HRTEM images evidence that good crystallinity and LMO crystal structure is remains.

DOI: 10.1038/NMAT4479

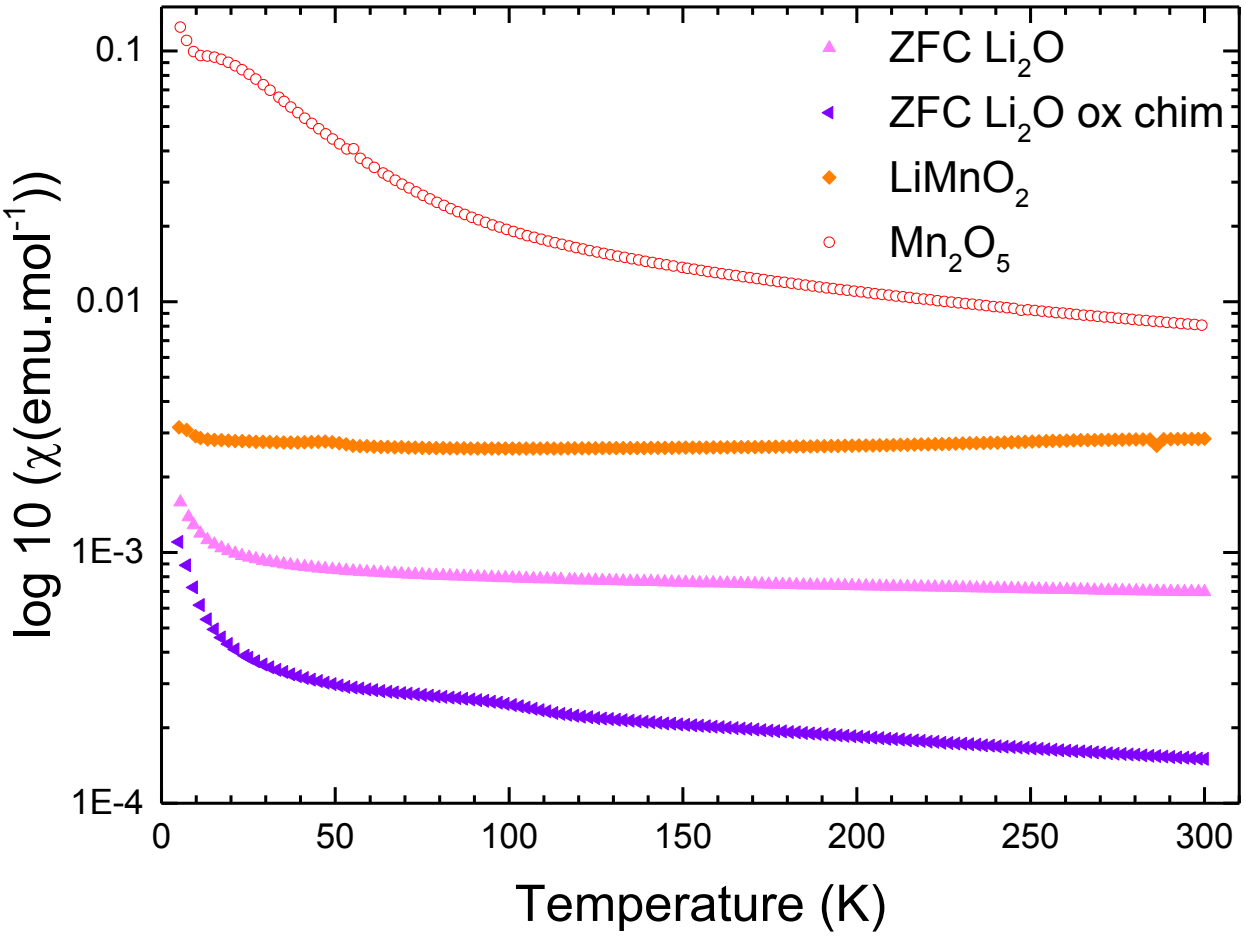

Figure S5. Comparison of the magnetic susceptibility of $Li_4Mn_2O_5$ chemically oxidized 'Mn_2O_5', Li_2O and Li_2O chemically oxidized, and $LiMnO_2$. Magnetic measurements, especially susceptibility χ measurements in the same conditions (between 5 and 300K, with a field equal to 0.1T), realized on Li_2O (after 40 hours of ball milling), Li_2O chemically oxidized with NO_2BF_4 and on orthorhombic $LiMnO_2$ (in pink, purple and orange, respectively). We note that these three paramagnetic phases do not follow the Curie-Weiss-like temperature dependence and have a week magnetic response (susceptibility around 10^{-3} and 10^{-4} emu.mol^{-1}) in comparison with the paramagnetic $Li_4Mn_2O_5$ chemically oxidized with NO_2BF_4, called 'Mn_2O_5'. This latter material 'Mn_2O_5' shows in the inverse of susceptibility χ^{-1}, a Curie-Weiss-like temperature dependence starting from ≈100K. Thus, even if Li_2O and $LiMnO_2$ are hypothetically formed after the electrochemical/chemical charge of $Li_4Mn_2O_5$, these decomposition products seem not having a large impact on the magnetic measurements.

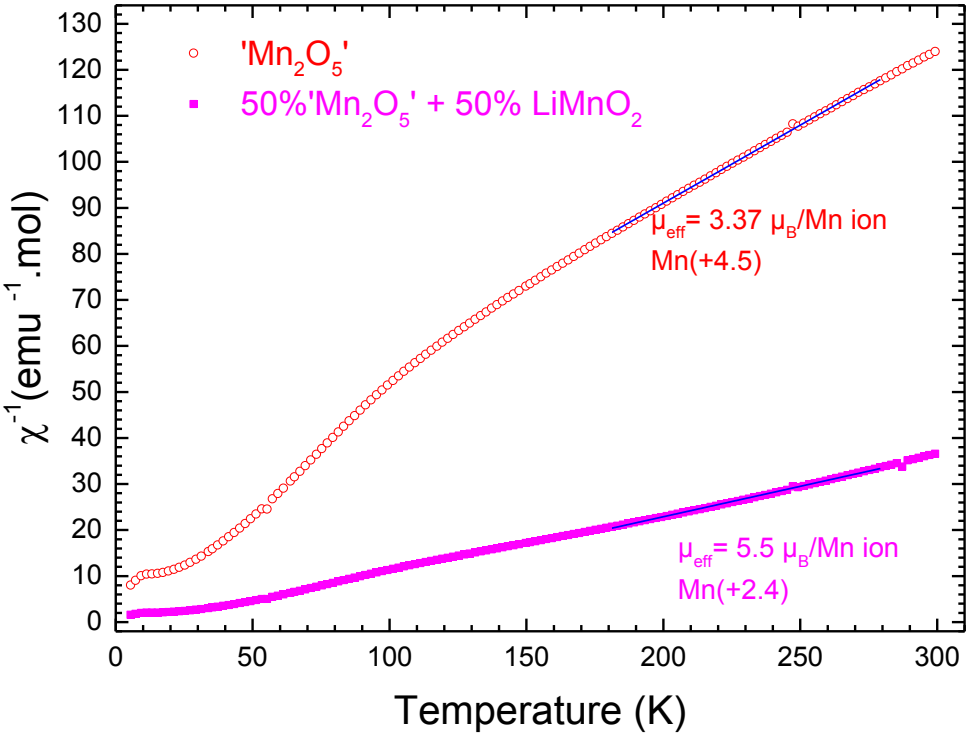

Figure S6. Comparison of the inverse of the magnetic susceptibility of $Li_4Mn_2O_5$ chemically oxidized 'Mn_2O_5' and (50% 'Mn_2O_5' + 50% $LiMnO_2$). Some simulations about an eventual decomposition of $Li_4Mn_2O_5$ in $LiMnO_2$ have been performed. Hypothetically, we have supposed that after oxidation of $Li_4Mn_2O_5$, we obtain 50% of 'Mn_2O_5' and 50% of $LiMnO_2$, instead of 100% of 'Mn_2O_5'. The presence of $LiMnO_2$ in the oxidized 'Mn_2O_5' material does not allow one to obtain a manganese oxidation state superior to +2.4. Therefore we can consider that the magnetic response of the fully oxidized phase 'Mn_2O_5' is mostly due to the manganese ions Mn^{4+}/Mn^{5+}.